Family of Mn(2)(III)Ln(2)(mu(4)-O) Compounds: Syntheses, Structures, and Magnetic Properties

ARTICLE *in* INORGANIC CHEMISTRY · JUNE 2010

Impact Factor: 4.76 · DOI: 10.1021/ic100373r · Source: PubMed

Inorganic Chemistry
Article

Inorg. Chem. **2010**, *49*, 5293–5302 **5293**
DOI: 10.1021/ic100373r

Family of $Mn^{III}_2Ln_2(\mu_4\text{-}O)$ Compounds: Syntheses, Structures, and Magnetic Properties

Valeriu Mereacre,[†] Yanhua Lan,[†] Rodolphe Clérac,[§,∥] Ayuk M. Ako,[†,‡] Ian J. Hewitt,[†] Wolfgang Wernsdorfer,[⊥] Gernot Buth,[⊗] Christopher E. Anson,[†] and Annie K. Powell*[,†,‡]

[†]*Institute of Inorganic Chemistry, Karlsruhe Institute of Technology, Engesserstrasse 15, D-76131, Karlsruhe, Germany,* [‡]*Institute of Nanotechnology, Karlsruhe Institute of Technology, Postfach 3640, D-76021 Karlsruhe, Germany,* [§]*CNRS, UPR 8641, Centre de Recherche Paul Pascal (CRPP), Equipe "Matériaux Moléculaires Magnétiques", 115 avenue du Dr. Albert Schweitzer, Pessac, F-33600, France,* [∥]*Université de Bordeaux, UPR 8641, Pessac, F-33600, France,* [⊥]*Institut Néel − CNRS, BP 166, 25 Avenue des Martyrs, 38042 Grenoble Cedex 9, France, and* [⊗]*Institut für Synchrotronstrahlung, Karlsruhe Insitute of Technology, D-76344 Eggenstein-Leopoldshafen, Germany*

Received February 24, 2010

An isostructural family of tetranuclear aggregates $[Mn^{III}_2Ln_2(O)(Piv)_2(hep)_4(NO_3)_4]\cdot MeCN$ (where Ln = Y^{III} (**1**), Pr^{III} (**2**), Nd^{III} (**3**), Gd^{III} (**4**), Tb^{III} (**5**), Dy^{III} (**6**), Ho^{III} (**7**), and Yb^{III} (**8**)) is reported. They were obtained from the reactions of 2-(2-hydroxyethyl)pyridine (hepH) with a preformed hexanuclear manganese complex, $[Mn_6]$, and the respective lanthanide salt. The complexes are isomorphous and represent a new heterometallic 3d-4f complex type for this class of ligand. The structural core of **1**−**8** consists of a distorted Mn_2Ln_2 tetrahedron with the four metal centers linking through a μ_4-O^{2-} bridging atom. The magnetic properties of all complexes were investigated by variable temperature magnetic susceptibility and magnetization measurements. The magnetic data of all compounds suggest that antiferromagnetic interactions are present between adjacent paramagnetic centers. Complexes **5**−**7** containing highly anisotropic lanthanide ions (Tb, Dy, and Ho) show slow relaxation of their magnetization.

Introduction

The design and synthesis of high-nuclearity transition metal complexes of paramagnetic ions with unusual magnetic properties is attracting increasing attention since the discovery that such molecules can behave as single-molecule magnets (SMMs).[1] Although the search for new and better SMMs has mainly focused on coordination clusters of 3d metals ions,[2−5] the incorporation of lanthanide ions into such molecules has recently been recognized as a route to new candidates for SMM behavior.[6−11] The inherent anisotropy of most lanthanide ions and the difficulty in analyzing the magnetic properties of 3d-4f couples makes the description of their magnetic properties challenging. This often makes identifying the origin of the SMM behavior in such compounds more complicated than is the case for coordination clusters based solely on 3d metal ions. Nevertheless, the use of lanthanide ions is appealing since there is the possibility of combining large spin states with the highly anisotropic nature of most of the single ions. Furthermore, the systematic study of a family 3d-4f compounds can lead to insights regarding the contributions to the overall magnetic behavior provided by a given lanthanide ion. For example, the Tb^{III} ion is a source of six electrons and significant anisotropy. Replacement of Tb^{III} with Gd^{III} can add an additional electron, but

*To whom correspondence should be addressed. E-mail: annie.powell@kit.edu. Fax: +49-721-608-8142. Phone: +49-721-608-2135.

(1) (a) Tsai, H.-L.; Schake, A. R.; Wang, S.; Vincent, J. B.; Folting, K.; Gatteschi, D.; Christou, G.; Hendrickson, D. N. *J. Am. Chem. Soc.* **1993**, *115*, 1804. (b) Sessoli, R.; Gatteschi, D.; Ganeschi, A.; Novak, M. A. *Nature* **1993**, *365*, 141.

(2) (a) Christou, G.; Gatteschi, D.; Hendrickson, D. N.; Sessoli, R. *MRS Bull.* **2000**, *25*, 66. (b) Price, J. P.; Batten, S. R.; Moubaraki, B.; Murray, K. S. *Chem. Commun.* **2002**, 762. (c) Sañudo, E. C.; Wernsdorfer, W.; Abboud, K. A.; Christou, G. *Inorg. Chem.* **2004**, *43*, 4137. (d) Chakov, N. E.; Wernsdorfer, W.; Abboud, K. A.; Christou, G. *Inorg. Chem.* **2004**, *43*, 5919. (e) Milios, C. J.; Raptopoulou, C. P.; Terzis, A.; Lloret, F.; Vicente, R.; Perlepes, S. P.; Escuer, A. *Angew. Chem., Int. Ed.* **2004**, *43*, 210. (f) Coronado, E.; Forment-Aliaga, A.; Gaita-Arino, A.; Gimenez-Saiz, C.; Romero, F. M.; Wernsdorfer, W. *Angew. Chem., Int. Ed.* **2004**, *45*, 6152. (g) Murugesu, M.; Habrych, M.; Wernsdorfer, W.; Abboud, K. A.; Christou, G. *J. Am. Chem. Soc.* **2004**, *126*, 4766. (h) Maheswaran, S.; Chastanet, G.; Teat, S. J.; Mallah, T.; Sessoli, R.; Wernsdorfer., W.; Winpenny, R. E. P. *Angew. Chem.* **2005**, *117*, 5172. (i) Boudalis, A. K.; Donnadieu, B.; Nastopoulos, V.; Clemente-Juan, J. M.; Mari, A.; Sanakis, Y.; Tuchagues, J.-P.; Perlepes, S. P. *Angew. Chem., Int. Ed.* **2004**, *43*, 2266. (j) Boudalis, A. K.; Raptopoulou, C. P.; Abarca, B.; Ballesteros, R.; Chadlaoui, M.; Tuchagues, J.-P.; Terzis, A. *Angew. Chem., Int. Ed.* **2006**, *45*, 432. (k) Brechin, E. K.; Boskovic, C.; Wernsdorfer, W.; Yoo, J.; Yamaguchi, A.; Sanudo, E. C.; Concolino, T. R.; Rheingold, A. L.; Ishimoto, H.; Hendrickson, D. N.; Christou, G. *J. Am. Chem. Soc.* **2002**, *124*, 9710. (l) Boskovic, C.; Brechin, E. K.; Streib, W. E.; Folting, K.; Bollinger, J. C.; Hendrickson, D. N.; Christou, G. *J. Am. Chem. Soc.* **2002**, *124*, 3725.

Published on Web 04/26/2010

largely switch off the Ln^{III} spin−orbit coupling effects and anisotropy. Introducing diamagnetic rare earths such as La^{III}, Y^{III}, or Lu^{III} can switch off the contribution from unpaired f-electrons altogether. However, a fundamental problem in much of the work reported on 3d-4f systems is the lack of systematic magnetic studies on a family of isostructural aggregates in which the 4f ion is varied across the series. Such an investigation could help provide answers to questions concerning, for example, the relative contributions of the 3d- and 4f ions to the magnetic properties of the molecule. It should also be possible to estimate how significant the interactions between the 3d- and 4f ions are or, indeed, whether these contributions to the overall magnetic behavior are largely independent. It should also be possible to discover the rules to help choose the best lanthanide to optimize the magnetic properties of a cluster. Thus, as an extension of our previous work on the synthesis of Mn-Ln complexes,[11a−i] we report here on the use of the ligand 2-(2-hydroxyethyl)pyridine (hepH) to access an isostructural family of Mn_2Ln_2 compounds running across the lanthanide series from Pr to Yb allowing us to address these issues. Although the hepH ligand has been widely used in manganese coordination chemistry affording high nuclearity manganese clusters with various Mn_x topologies,[2j,k] the potential of this ligand does not seem to have been fully exploited in transition metal−lanthanide coordination chemistry. We present the syntheses, structures, and magnetic properties of a [Mn-Ln] family of compounds with the general formula: $[Mn_2Ln_2(O)(Piv)_2(hep)_4(NO_3)_4]\cdot MeCN$ (where Ln = Y^{III} (**1**), Pr^{III} (**2**), Nd^{III} (**3**), Gd^{III} (**4**), Tb^{III} (**5**), Dy^{III} (**6**), Ho^{III} (**7**), and Yb^{III} (**8**), Piv = pivalate anions).

Experimental Section

General Procedures. Unless otherwise stated, all reagents were obtained from commercial sources and were used as received, without further purification. All reactions were carried out under aerobic conditions. Elemental analyses on C, H, and N were performed using an Elementar Vario EL analyzer, and carried out at the Institute of Inorganic Chemistry, Karlsruhe Institute of Technology. IR spectra were measured on a Perkin-Elmer Spectrum One spectrometer with samples prepared as KBr disks. $[Mn_6O_2(Piv)_{10}(4\text{-Me-py})_{2.5}(PivH)_{1.5}]$ was synthesized as described elsewhere.[11a]

Preparation of 1−8. $Ln(NO_3)_3\cdot 6H_2O$ (0.88 mmol) was added to a stirred slurry of $[Mn_6O_2(Piv)_{10}(4\text{-Me-py})_{2.5}(PivH)_{1.5}]$ (0.20 g, 0.11 mmol) and 2-(2-hydroxyethyl) pyridine (0.22 g, 1.80 mmol) in MeCN (15 mL). The solution immediately became green and was stirred for a further 5 min at room temperature. (It should be noted that if the solution is stirred for more than 5 min, a light green precipitate starts forming). The green-brown solution was filtered and left undisturbed for 6 h during which time green-brown crystals began to form. After 2 days the fully grown crystals were collected by filtration, washed with 5 mL cold MeCN, and dried in air.

Yield (based on Mn): 39% for **1**; 40% for **2**; 35% for **3**; 32% for **4**; 31% for **5**; 42% for **6**; 37% for **7**; 38% for **8**. Elemental analysis calcd (%) for $C_{38}H_{50}N_8O_{21}Mn_2Y_2$ (**1**) (dried): C, 36.73; H, 4.05; N 9.02. Found: C, 36.71; H, 4.23; N, 8.88. IR (KBr, cm^{-1}): ν = 2961 (w), 2922 (m), 1607 (w), 1569 (m), 1558 (m), 1483 (vs), 1445 (m), 1420(m), 1372 (m), 1319 (s), 1311 (s), 1225 (w), 1160 (w), 1108 (w), 1072 (s), 1032 (s), 981 (w), 863 (w), 817 (w), 791 (m), 769 (w), 744 (w), 655 (m), 600 (m), 581 (m), 546 (w), 510 (w), 432 (w). Anal. Calcd (%) for $C_{38}H_{50}N_8O_{21}Mn_2Pr_2$ (**2**) (dried): C, 33.89; H, 3.74; N 8.32. Found: C, 33.73; H, 3.63; N, 8.17. IR (KBr, cm^{-1}): ν = 2962 (w), 2930 (m), 1606 (w), 1576 (m), 1555 (m), 1485 (vs), 1447 (m), 1416 (m), 1380 (m), 1321 (s), 1313 (s), 1224 (w), 1164 (w), 1110 (w), 1069 (s), 1034 (s), 981 (w), 866 (w), 820 (w), 790 (m), 767 (w), 743 (w), 660 (m), 597 (m), 583 (m), 544 (w), 507 (w), 434 (w). Anal. Calcd (%) for $C_{38}H_{50}N_8O_{21}Mn_2Nd_2$ (**3**) (dried): C, 33.72; H, 3.72; N 8.28. Found: C, 33.85; H, 3.58; N, 8.05. IR (KBr, cm^{-1}): ν = 2963 (w), 2927 (m), 1607 (w), 1572 (m), 1555 (m), 1484 (vs), 1442 (m), 1421 (m), 1380 (m), 1322 (s), 1311 (s), 1223 (w), 1166 (w), 1109 (w), 1073 (s), 1035 (s), 976 (w), 865 (w), 817 (w), 788 (m), 765 (w), 742 (w), 659 (m), 597 (m), 581 (m), 546 (w), 506 (w), 432 (w). Anal. Calcd (%) for $C_{38}H_{50}N_8O_{21}Mn_2Gd_2$ (**4**) (dried): C, 33.09; H, 3.65; N 8.12. Found: C, 32.91; H, 3.53; N, 7.98. IR (KBr, cm^{-1}): ν = 2960 (w), 2926 (m), 1606 (w), 1574 (m), 1560 (m), 1482 (vs), 1447 (m), 1417 (m), 1373 (m), 1320 (s), 1313 (s), 1226 (w), 1161 (w), 1109 (w), 1073 (s), 1036 (s), 981 (w), 864 (w), 813 (w), 789 (m), 767 (w), 741 (w), 659 (m), 597 (m), 585 (m), 549 (w), 505 (w), 434 (w). Anal. Calcd (%) for $C_{38}H_{50}N_8O_{21}Mn_2Tb_2$ (**5**) (dried): C, 33.01; H, 3.64; N 8.10. Found: C, 32.91; H, 3.51; N, 7.92. IR (KBr, cm^{-1}): ν = 2960 (w), 2926 (m), 1604 (w), 1573 (m), 1560 (m), 1481 (vs), 1445 (m), 1420 (m), 1376 (m), 1319 (s), 1312 (s), 1224 (w), 1161 (w), 1108 (w), 1072 (s), 1035 (s), 979 (w), 867 (w), 813 (w), 790 (m), 770 (w), 741 (w), 657 (m), 600 (m), 582 (m), 549 (w), 506 (w), 430 (w). Anal. Calcd (%) for $C_{38}H_{50}N_8O_{21}Mn_2Dy_2$ (**6**) (dried): C, 32.84; H, 3.62; N 8.06. Found: C, 32.71; H, 3.53; N, 7.88. IR

(3) (a) Delfs, C.; Gatteschi, D.; Pardi, L.; Sessoli, R.; Wieghardt, K.; Hanke, D. *Inorg. Chem.* **1993**, *32*, 3099. (b) Gatteschi, D.; Sessoli, R.; Cornia, A. *Chem. Commun.* **2000**, 725. (c) Goodwin, J. C.; Sessoli, R.; Gatteschi, D.; Wernsdorfer, W.; Powell, A. K.; Heath, S. L. *J. Chem. Soc., Dalton Trans.* **2000**, 1835. (d) Benelli, C.; Cano, J.; Journaux, Y.; Sessoli, R.; Solan, G. A.; Winpenny, R. E. P. *Inorg. Chem.* **2001**, *40*, 188.

(4) (a) Cadiou, C.; Murrie, M.; Paulsen, C.; Villar, V.; Wernsdorfer, W.; Winpenny, R. E. P. *Chem. Commun.* **2001**, 2666. (b) Nakano, M.; Matsubayashi, G.-E.; Takaki, M.; Tatsuo, C. K.; Amaya, K.; Yoo, J.; Christou, G.; Hendrickson, D. N. *Mol. Cryst. Liq. Cryst. Sci. Technol., Sect. A* **2002**, *376*, 405. (c) Ochsenbein, S. T.; Murrie, M.; Rusanov, E.; Stoeckli-Evans, H.; Sekine, C.; Güdel, H. U. *Inorg. Chem.* **2002**, *41*, 5133.

(5) (a) Yang, E.-C.; Hendrickson, D. N.; Wernsdorfer, W.; Nakano, M.; Zakharov, L. N.; Sommer, R. D.; Rheingold, A. L.; Ledezma-Gairaud, M.; Christou, G. *J. Appl. Phys.* **2002**, *91*, 7382. (b) Murrie, M.; Teat, S. J.; Stoeckli-Evans, H.; Güdel, H. U. *Angew. Chem., Int. Ed.* **2003**, *42*, 4653.

(6) (a) Osa, S.; Kido, T.; Matsumoto, N.; Re, N.; Pochaba, A.; Mrozinski, J. *J. Am. Chem. Soc.* **2004**, *126*, 420. (b) Mori, F.; Nyui, T.; Ishida, T.; Nogami, T.; Choi, K.-Y.; Nojiri, H. *J. Am. Chem. Soc.* **2006**, *128*, 1440. (c) Pointillart, F.; Bernot, K.; Sessoli, R.; Gatteschi, D. *Chem.—Eur. J.* **2007**, *13*, 1602. (d) Shiga, T.; Onuki, T.; Matsumoto, T.; Nojiri, H.; Newton, G. N.; Hoshino, N.; Oshio, H. *Chem. Commun.* **2009**, 3568. (e) Sessoli, R.; Powell, A. K. *Coord. Chem. Rev.* **2009**, *253*, 2328.

(7) Zaleski, C.; Depperman, E.; Kampf, J.; Kirk, M.; Pecoraro, V. *Angew. Chem., Int. Ed.* **2004**, *43*, 3912.

(8) (a) Mishra, A.; Wernsdorfer, W.; Abboud, K.; Christou, G. *J. Am. Chem. Soc.* **2004**, *126*, 15648. (b) Stamatatos, T. C.; Teat, S. J.; Wernsdorfer, W.; Christou, G. *Angew. Chem., Int. Ed.* **2009**, *48*, 521.

(9) Mishra, A.; Wernsdorfer, W.; Parson, S.; Christou, G.; Brechin, E. *Chem. Commun.* **2005**, 2086.

(10) Murugesu, M.; Mishra, A.; Wernsdorfer, W.; Abboud, K.; Christou, G. *Polyhedron* **2006**, *26*, 613.

(11) (a) Mereacre, V.; Ako, A. M.; Clérac, R.; Wernsdorfer, W.; Filoti, G.; Bartolomé, J.; Anson, C. E.; Powell, A. K. *J. Am. Chem. Soc.* **2007**, *129*, 9248. (b) Mereacre, V.; Ako, A. M.; Clérac, R.; Wernsdorfer, W.; Hewitt, I. J.; Anson, C. E.; Powell, A. K. *Chem.—Eur. J.* **2008**, *14*, 3577. (c) Mereacre, V.; Prodius, D.; Ako, A. M.; Kaur, N.; Lipkowski, J.; Simmons, C.; Dalal, N.; Geru, I.; Anson, C. E.; Powell, A. K.; Turta, C. *Polyhedron* **2008**, *27*, 2459. (d) Ako, A. M.; Mereacre, V.; Clérac, R.; Hewitt, I. J.; Lan, Y.; Buth, G.; Anson, C. E.; Powell, A. K. *Inorg. Chem.* **2009**, *48*, 6713. (e) Akhtar, M. N.; Lan, Y.; Mereacre, V.; Clérac, R.; Anson, C. E.; Powell, A. K. *Polyhedron* **2009**, *28*, 1698. (f) Ako, A. M.; Mereacre, V.; Clérac, R.; Wernsdorfer, W.; Hewitt, I. J.; Anson, C. E.; Powell, A. K. *Chem. Commun.* **2009**, 544. (g) Akhtar, M. N.; Zheng, Y.-Z.; Lan, Y.; Mereacre, V.; Anson, C. E.; Powell, A. K. *Inorg. Chem.* **2009**, *48*, 3502. (h) Mereacre, V.; Ako, A. M.; Filoti, G.; Bartolomé, J.; Anson, C. E.; Powell, A. K. *Polyhedron* **2009**, *1*, 244. (i) Mereacre, V.; Ako, A. M.; Akhtar, M. N.; Lindemann, A.; Anson, C. E.; Powell, A. K. *Helv. Chim. Acta* **2009**, *92*, 2507. (j) Abbas, G.; Lan, Y.; Mereacre, V.; Wernsdorfer, W.; Clérac, R.; Buth, G.; Sougrati, M. T.; Grandjean, F.; Long, G. J.; Anson, C. E.; Powell, A. K. *Inorg. Chem.* **2009**, *48*, 9345. (k) Akhtar, M. N.; Mereacre, V.; Novitchi, G.; Tuchagues, J.-P.; Anson, C. E.; Powell, A. K. *Chem.—Eur. J.* **2009**, *30*, 7278.

(KBr, cm^{-1}): ν = 2959 (w), 2926 (m), 1605 (w), 1571 (m), 1557 (m), 1483 (vs), 1444 (m), 1419 (m), 1375 (m), 1321 (s), 1311 (s), 1224 (w), 1162 (w), 1107 (w), 1071 (s), 1034 (s), 979 (w), 865 (w), 816 (w), 789 (m), 769 (w), 743 (w), 658 (m), 598 (m), 582 (m), 548 (w), 509 (w), 430 (w). Anal. Calcd (%) for $C_{38}H_{50}N_8O_{21}Mn_2Ho_2$ (**7**) (dried): C, 32.72; H, 3.61; N 8.03. Found: C, 32.78; H, 3.43; N, 7.83. IR (KBr, cm^{-1}): ν = 2963 (w), 2930 (m), 1603 (w), 1574 (m), 1557 (m), 1484 (vs), 1447 (m), 1417 (m), 1373 (m), 1322 (s), 1312 (s), 1222 (w), 1160 (w), 1106 (w), 1068 (s), 1035 (s), 977 (w), 863 (w), 814 (w), 786 (m), 771 (w), 741 (w), 659 (m), 594 (m), 586 (m), 549 (w), 512 (w), 427 (w). Anal. Calcd (%) for $C_{38}H_{50}N_8O_{21}Mn_2Yb_2$ (**8**) (dried): C, 32.35; H, 3.57; N 7.94. Found: C, 32.47; H, 3.43; N, 8.15. IR (KBr, cm^{-1}): ν = 2959 (w), 2928 (m), 1607 (w), 1572 (m), 1555 (m), 1484 (vs), 1439 (m), 1419 (m), 1377 (m), 1322 (s), 1314 (s), 1221 (w), 1161 (w), 1109 (w), 1069 (s), 1032 (s), 981 (w), 866 (w), 817 (w), 788 (m), 768 (w), 743 (w), 657 (m), 596 (m), 581 (m), 548 (w), 510 (w), 431 (w).

X-ray Crystallography. For compounds **1**−**6**, the data were collected at 100 K with graphite-monochromated Mo−Kα radiation, using a Bruker SMART Apex (**1**−**3**, **5**, **6**) or Oxford Xcalibur Gemini R (**4**) CCD diffractometer. Compounds **7** and **8** were measured to 0.85 Å resolution at 150 K on the ANKA-SCD synchrotron beamline at the Karlsruhe Institute of Technology with λ = 0.8000 Å radiation using a Stoe IPDS II image plate diffractometer. For **7** and **8**, f' and f'' were obtained from http://skuld.bmsc.washington.edu/scatter/AS_periodic.html, and absorption coefficients from http://www.csrri.iit.edu/periodic-table.html. Crystallographic details and details of the data collection are summarized in Table 1. Absorption corrections were made using SADABS[12a] (**1**−**3**, **5**, **6**), ABSPACK[12b] (**4**) or XPREP in SHELXTL[12c] (**8**). The structures were solved using direct methods, followed by full-matrix least-squares refinement against F^2 (all data) using SHELXTL.[12c] Anisotropic refinement was used for all ordered non-H atoms; organic H atoms were placed in calculated positions. In all compounds, the *t*-butyl group of one pivalate ligand and the lattice MeCN showed two- or 3-fold disorder; these were refined using partial C and N atoms, with geometrical restraints as appropriate.

Crystallographic data (excluding structure factors) for the structures in this paper have been deposited with the Cambridge Crystallographic Data Centre as supplementary publication nos. CCDC 758178−758185. Copies of the data can be obtained, free of charge, on application to CCDC, 12 Union Road, Cambridge CB2 1EZ, U.K.: http://www.ccdc.cam.ac.uk/cgi-bin/catreq.cgi, e-mail: data_request@ccdc.cam.ac.uk, or fax: +44 1223 336033.

Magnetic Measurements. The magnetic susceptibility measurements were obtained using a Quantum Design SQUID magnetometer MPMS-XL. This magnetometer works between 1.8 and 400 K for direct current (dc) applied fields ranging from −7 to 7 T. Measurements were performed on a polycrystalline sample of 6.58, 23.76, 16.18, 17.61, 15.69, and 20.16 mg for **1**, **4**, **5**, **6**, **7**, and **8**, respectively. Alternating current (ac) susceptibility measurements were performed with an oscillating field of 3 Oe and ac frequencies ranging from 1 to 1500 Hz. *M* versus *H* measurements were performed at 100 K to check for the presence of ferromagnetic impurities which were found to be absent. The magnetic data were corrected for the sample holder and the diamagnetic contribution. Magnetization measurements on oriented single crystals were carried out using an array of micro-SQUIDs,[13] working in the temperature range of 0.04 to about 7 K and in fields of up to 0.8 T with sweeping rates as high as 0.28 T s^{-1}, and exhibiting field stability of better than 1 μT. The time resolution is approximately 1 ms, and the field can be applied in any direction of the micro-SQUID plane with precision better than 0.1° by separately driving three orthogonal coils. To ensure good thermalization, a single crystal was fixed with apiezon grease.

Results and Discussion

Syntheses. Although a variety of structural types and compositions have been identified so far for Mn-Ln clusters, there are only few reports of high (≥4) nuclearity Mn-Ln complexes,[6−11] and it is of interest to develop new synthetic strategies to incorporate rare-earth metals into manganese systems. Furthermore, many high nuclearity hybrid lanthanide-Mn complexes present beautiful and intriguing structural architectures of inherent interest in coordination chemistry. Among the various strategies used in the synthesis of Mn-4f complexes, those using simple manganese salts or preformed small nuclearity species with $[Mn_3O]^{6+/7+}$ or $[Mn_4O_2]^{8+}$ cores are proving fruitful. In this way, the hexanuclear mixed-valent $Mn^{III}Mn^{II}$ complex $[Mn_6(O)_2(Piv)_{10}(THF)_4]$ has already been shown to be useful,[14] but we believe that the potential of this compound has not been fully exploited, since only a few complexes derived from this complex have been reported in the literature.[15,16] Recently we reported the synthesis of Mn-Ln complexes using a similar hexanuclear manganese $[Mn_6O_2(Piv)_{10}(4\text{-Me-py})_{2.5}(PivH)_{1.5}]$, which resulted in a series of high-nuclearity compounds $[Mn^{III}_9Mn^{II}_2Gd_2(O)_8(OH)_2(Piv)_{10.6}(fca)_{6.4}(NO_3)_2(H_2O)]$,[11a] $[Mn_5Ln_4(O)_6(mdea)_2(mdeaH)_2(Piv)_6(NO_3)_4(H_2O)_2]\cdot 2MeCN$ (Ln = Tb, Dy, Ho and Y),[11b] and $[Mn_4Nd_4(OH)_4(fcdc)_2(Piv)_8(n\text{-bdea})_4]$.[11h]

In the work we report here, reaction of $[Mn_6O_2(Piv)_{10}(4\text{-Me-py})_{2.5}(PivH)_{1.5}]$, hepH, and $Ln(NO_3)_3\cdot 6H_2O$ in a 1:16:8 molar ratio in MeCN at room temperature gave a dark-green solution from which green-brown crystals of $[Mn_2Ln_2(O)(Piv)_2(hep)_4(NO_3)_4]\cdot$MeCN (where Ln = Y^{III} (**1**), Pr^{III} (**2**), Nd^{III} (**3**), Gd^{III} (**4**), Tb^{III} (**5**), Dy^{III} (**6**), Ho^{III} (**7**), and Yb^{III} (**8**)) began to crystallize after 6 h with fully grown crystals in good yield and suitable for X-ray crystal structure studies were available after only 2 days. While the synthetic procedure presented herein is reproducible for all lanthanides from Pr to Yb, the reaction with $Ce(NO_3)_3\cdot 6H_2O$ gave a much larger aggregate $[Ce^{IV}_6Mn^{III}_8(\mu_4\text{-}O)_4(\mu_3\text{-}O)_8(hep)_4(Piv)_{18}]_2[Ce^{IV}_6(\mu_3\text{-}O)_4(\mu_3\text{−}OH)_4(Piv)_{10}(NO_3)_4(OAc)_2][Ce^{III}(NO_3)_5(H_2O)]\cdot 21MeCN$ (**9**) with most of the Ce^{III} being oxidized to Ce^{IV} (See Supporting Information) which we have reported elsewhere.[11i] This is the first Mn^{III}_x-Ce^{IV}_y (where x or y > 1) aggregate in which all manganese ions are in oxidation state III and cerium ions are in oxidation state IV starting from Ce^{III} rather than Ce^{IV}.[17]

Description of Crystal Structures of 1−8. X-ray single crystal analysis revealed that compounds **1**−**8** are isomorphous presenting a distorted $[Mn^{III}_2Ln_2]$ tetrahedron

(12) (a) Sheldrick, G. M. *SADABS, the Siemens Area Detector Absorption Correction*; University of Göttingen: Göttingen, Germany, 1996. (b) *ABSPACK, Oxford Diffraction*; Abingdon, U.K., 1996. (c) Sheldrick, G. M. *SHELXTL 6.14*, Bruker AXS, Inc., Madison, WI, 2003.

(13) Wernsdorfer, W. *Adv. Chem. Phys.* **2001**, *118*, 99.

(14) Benelli, C.; Murrie, M.; Parsons, S.; Winpenny, R. *J. Chem. Soc., Dalton Trans.* **1999**, 4125.

(15) Murrie, M.; Parsons, S.; Winpenny, R. *J. Chem. Soc., Dalton Trans.* **1998**, 1423.

(16) Fursova, E.; Ovcharenko, V.; Nosova, K.; Romanenko, G.; Ikorskii, V. *Polyhedron* **2005**, *24*, 2084.

(17) (a) Tasiopoulos, A. J.; O'Brien, T. A.; Abboud, K. A.; Christou, G. *Angew. Chem., Int. Ed.* **2004**, *43*, 345. (b) Tasiopoulos, A. J.; Mishra, A.; Christou, G. *Polyhedron* **2007**, *26*, 2183.

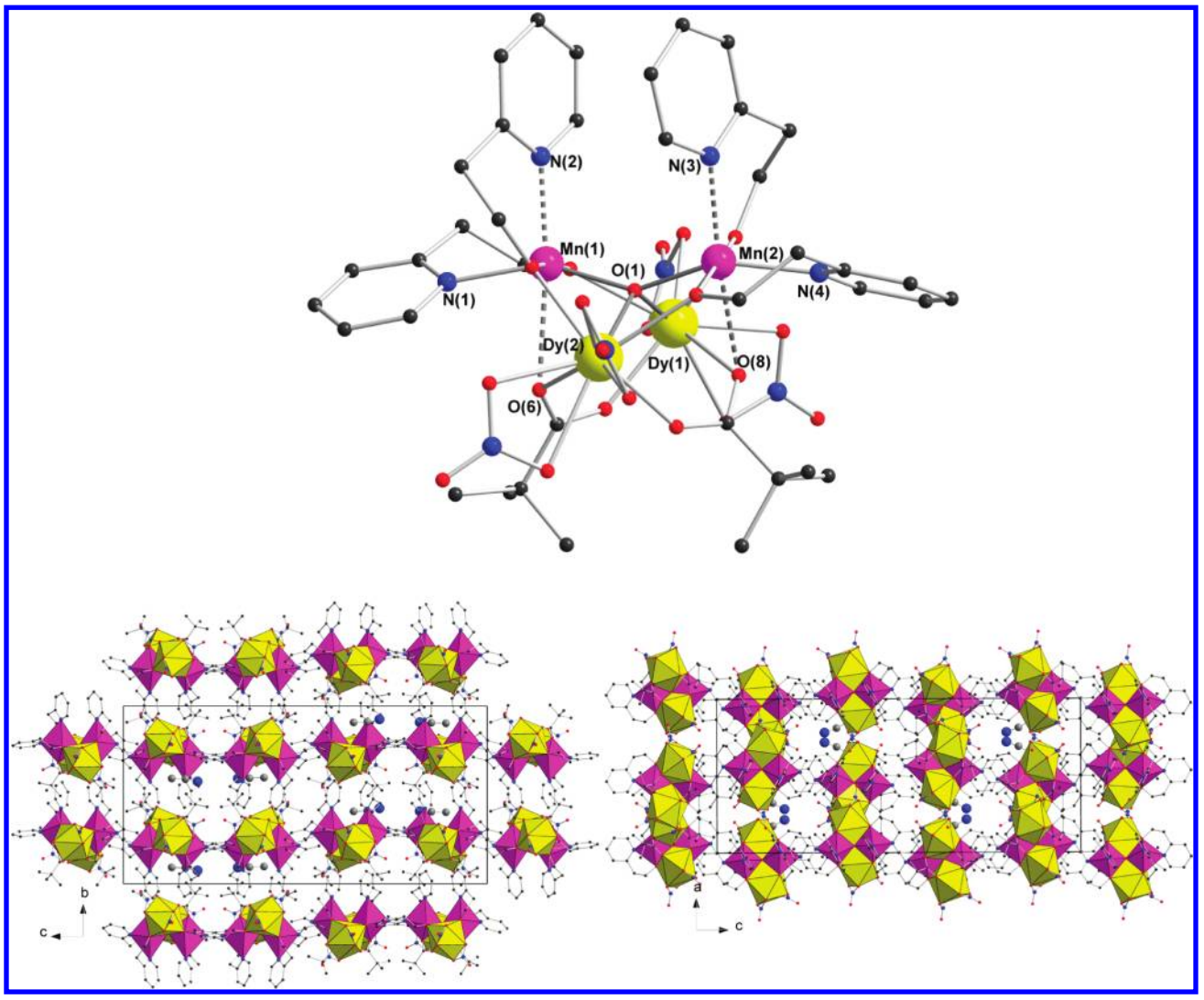

Figure 1. Molecular structure of $[Mn_2Dy_2(O)(hep)_4(Piv)_2(NO_3)_4]$ (**6**) (above) and packing in the crystal structure of **6** viewed along the *a*-axis (below, left) and *b*-axis (below, right). The metal coordination environments are shown as polyhedra (Dy^{III} yellow and Mn^{III} pink). Hydrogen atoms have been omitted for clarity.

topology. A view of **6** is shown in Figure 1, and a full description of its structure given here as representative for the whole series. Selected metric parameters and bond distances and angles are summarized in Tables 1− 9. The Ln1−O1 and Ln2−O1 bond distances generally decrease in the order **2** > **3** > **4** > **5** > **6** > **7** > **8**, in accord with the lanthanide contraction (Figure 2). The average Mn1−O1 and Mn2−O1 distances vary from 1.907 to 1.926 Å and 1.891 to 1.898 Å, respectively. The Ln1−Ln2 and Mn(1,2)−Ln(1,2) separations are also in accord with the lanthanide contraction, although this is not the case for the Mn1−Mn2 separation and Mn1−O1−Mn2 and Ln1−O1−Ln2 angle (Table 10). Charge considerations, metric parameters, bond valence sums, and Jahn−Teller elongation axes were used to establish the oxidation state of the Mn ions. While a great many tetranuclear Mn[18] or Mn-4f [9,10,14] compounds presenting planar or butterfly topologies have been reported in the literature, the core of **1**−**8** is in general rare and unique for a tetranuclear $[Mn_2Ln_2]$ complex. To our knowledge, only a few examples of Mn_4 complexes with the same topology have been reported in recent times.[19] A salient structural feature of these compounds is that they represent the first example of a manganese−lanthanide tetranuclear complex with four metal centers interacting through a μ_4-O^{2-} bridging atom. The four vertices of the tetrahedron are bridged by

(18) (a) Yoo, J.; Yamaguchi, A.; Nakano, N.; Krystek, J.; Streib, W. E.; Brunel, L. C.; Ishimoto, H.; Christou, G.; Hendrickson, D. N. *Inorg. Chem.* **2001**, *40*, 4604. (b) Yang, E. C.; Harden, N.; Wernsdorfer, W.; Zakharov, L.; Brechin, E. K.; Rheingold, A. L.; Christou, G.; Hendrickson, D. N. *Polyhedron* **2003**, *22*, 1857. (c) Hendrickson, D. N.; Christou, G.; Ishimoto, H.; Yoo, J.; Brechin, E. K.; Yamaguchi, A.; Rumberger, E. M.; Aubin, S. M. J.; Sun, S.; Aromí, G. *Polyhedron* **2001**, *20*, 1479. (d) Brechin, E. K.; Yoo, J.; Nakano, M.; Huffman, J. C.; Hendrickson, D. N.; Christou, G. *Chem. Commun.* **1999**, 783. (e) Wittick, L. M.; Murray, K. S.; Moubaraki, B.; Batten, S. R.; Spiccia, L.; Berry, K. J. *Dalton Trans.* **2004**, 1003. (f) Foguet-Albiol, D.; O'Brien, T. A.; Wernsdorfer, W.; Moulton, B.; Zaworotko, M.; Abboud, K. A.; Christou, G. *Angew. Chem., Int. Ed.* **2005**, *44*, 897. (g) Ako, A. M.; Mereacre, V.; Hewitt, I. J.; Clérac, R.; Lecren, L.; Anson, C. E.; Powell, A. K. *J. Mater. Chem.* **2006**, *16*, 2579.

(19) (a) Afrati, T.; Dendrinou-Samara, C.; Raptopoulou, C. P.; Terzis, A.; Tangoulis, V.; Kessissoglou, D. P. *Angew. Chem.* **2002**, *114*, 2252. (b) McCrea, J.; McKee, V.; Metcalfe, T.; Tandon, S. S.; Wikaira, J. *Inorg. Chim. Acta* **2000**, *297*, 220. (c) Gallo, E.; Solari, E.; Angelis, S.; Floriani, C.; Re, N.; Chiesi-Villa, A.; Rizzoli, C. *J. Am. Chem. Soc.* **1993**, *115*, 9850. (d) Beagley, B.; McAuliffe, C. A.; Mac Rory, P. P.; Ndifon, P. T.; Pritchard, R. G. *J. Chem. Soc., Chem. Commun.* **1990**, 309. (e) Yang, C.-I.; Wernsdorfer, W.; Tsai, Y.-J.; Chung, G.; Kuo, T.-S.; Lee, G.-H.; Shieh, M.; Tsai, H.-L. *Inorg. Chem.* **2008**, *47*, 1925.

Table 1. Crystallographic Data and Structure Refinement for Complexes **1**−**8**

	1	**2**	**3**	**4**
formula	$C_{40}H_{53}Mn_2N_9O_{21}Y_2$	$C_{40}H_{53}Mn_2N_9O_{21}Pr_2$	$C_{40}H_{53}Mn_2N_9Nd_2O_{21}$	$C_{40}H_{53}Gd_2Mn_2N_9O_{21}$
M_r	1283.61	1387.61	1394.27	1420.29
crystal size [mm]	0.19 × 0.14 × 0.08	0.28 × 0.26 × 0.20	0.34 × 0.32 × 0.18	0.18 × 0.17 × 0.06
color	dichroic (blue/brown)	dichroic (blue/brown)	dichroic (blue/brown)	dichroic (blue/brown)
crystal system	orthorhombic	orthorhombic	orthorhombic	orthorhombic
space group	*Pbca*	*Pbca*	*Pbca*	*Pbca*
T [K]	100	100	100	100
a [Å]	15.6701(10)	15.7824(8)	15.8109(8)	15.7188(2)
b [Å]	17.9508(11)	18.0167(9)	18.0655(9)	17.9802(3)
c [Å]	36.833(2)	36.8863(17)	36.9519(18)	36.9802(6)
V [Å^3]	10360.7(11)	10488.5(9)	10554.6(9)	10412.5(3)
Z	8	8	8	8
ρ_{calcd} [g/cm^{-3}]	1.646	1.757	1.755	1.812
λ/Å	0.71073	0.71073	0.71073	0.71073
μ [mm^{-1}]	2.779	2.379	2.486	3.073
F(000)	5216	5536	5552	5616
reflections collected	42292	40880	47051	42757
unique reflections	9231	10307	10416	10923
R_{int}	0.1184	0.0528	0.0542	0.0521
refl. with [$I > 2\sigma(I)$]	4908	7526	8002	6485
parameters/restraints	693/16	696/21	700/13	670/4
GOF on F^2	0.791	0.995	1.014	1.023
R_1 [$I > 2\sigma(I)$]	0.0386	0.0393	0.0411	0.0362
wR_2 (all data)	0.0569	0.0718	0.0825	0.0869
largest residuals [e Å^{-3}]	+0.55/−0.48	+1.00/ −0.79	+1.16/−0.64	+2.20/−1.04
	5	**6**	**7**	**8**
formula	$C_{40}H_{53}N_9O_{21}Mn_2Tb_2$	$C_{40}H_{53}N_9O_{21}Mn_2Dy_2$	$C_{40}H_{53}N_9O_{21}Mn_2Ho_2$	$C_{40}H_{53}N_9O_{21}Mn_2Yb_2$
M_r	1423.63	1430.79	1435.65	1451.87
crystal size [mm]	0.17 × 0.12 × 0.09	0.24 × 0.21 × 0.19	0.07 × 0.04 × 0.02	0.025 × 0.015 × 0.010
color	dichroic (blue/brown)	dichroic (blue/brown)	dichroic (blue/brown)	dichroic (blue/brown)
crystal system	orthorhombic	orthorhombic	orthorhombic	orthorhombic
space group	*Pbca*	*Pbca*	*Pbca*	*Pbca*
T [K]	100	100	150	150
a [Å]	15.6934(8)	15.6516(13)	15.6530(5)	15.6185(4)
b [Å]	17.9446(9)	17.8928(15)	17.9691(4)	17.9341(4)
c [Å]	36.8186(19)	36.775(3)	36.8519(8)	36.7970(9)
V [Å^3]	10368.6 (9)	10298.8 (15)	10365.3 (5)	10307.0 (4)
Z	8	8	8	8
ρ_{calcd} [g/cm^{-3}]	1.824	1.846	1.840	1.871
λ/Å	0.71073	0.71073	0.8000	0.8000
μ [mm^{-1}]	3.255	3.433	4.805	5.597
F(000)	5632	5648	5664	5712
reflections collected	49401	50161	50349	50286
unique reflections	11176	11947	8432	8585
R_{int}	0.0433	0.0342	0.0740	0.0731
refl. with [$I > 2\sigma(I)$]	8559	9280	7623	7642
parameters/restraints	675/4	693/16	675/4	685/6
GOF on F^2	0.992	1.012	1.053	1.070
R_1 [$I > 2\sigma(I)$]	0.0280	0.0269	0.0360	0.0304
wR_2 (all data)	0.0531	0.0555	0.0860	0.0694
largest residuals [e Å^{-3}]	+0.93/−0.53	+1.06/−0.59	+0.80/−1.15	+0.69/−0.80

Table 2. Selected Bond Distances (Å) and Angles (deg) for Complex **1**

Bond Lengths			
Y1−O1	2.390(3)	Mn1−O6	2.583(3)
Y2−O1	2.418(3)	Mn2−O5	1.872(4)
Mn1−O2	1.867(3)	Mn2−O4	1.872(3)
Mn1−O3	1.869(3)	Mn2−O1	1.893(2)
Mn1−O1	1.915(2)	Mn2−N4	2.094(3)
Mn1−N1	2.087(3)	Mn2−N3	2.196(4)
Mn1−N2	2.175(3)	Mn2−O8	2.562(3)
Bond Angles			
Mn2−O1−Mn1	144.26(14)	Mn2−O1−Y2	101.92(11)
Mn2−O1−Y1	93.72(10)	Mn1−O1−Y2	92.45(10)
Mn1−O1−Y1	101.47(11)	Y1−O1−Y2	130.57(10)

Table 3. Selected Bond Distances (Å) and Angles (deg) for Complex **2**

Bond Lengths			
Pr1−O1	2.487(3)	Mn1−O6	2.638(3)
Pr2−O1	2.525(3)	Mn2−O5	1.879(3)
Mn1−O2	1.868(3)	Mn2−O4	1.876(3)
Mn1−O3	1.870(3)	Mn2−O1	1.896(3)
Mn1−O1	1.923(3)	Mn2−N4	2.090(4)
Mn1−N1	2.093(4)	Mn2−N3	2.198(4)
Mn1−N2	2.172(4)	Mn2−O8	2.616(3)
Bond Angles			
Mn2−O1−Mn1	145.62(16)	Mn2−O1−Pr2	101.92(11)
Mn2−O1−Pr1	93.99(11)	Mn1−O1−Pr2	92.45(10)
Mn1−O1−Pr1	101.13(12)	Pr1−O1−Pr2	128.72(12)

Table 4. Selected Bond Distances (Å) and Angles (deg) for Complex **3**

Bond Lengths			
Nd1−O1	2.480(3)	Mn1−O6	2.643(3)
Nd2−O1	2.519(3)	Mn2−O5	1.880(3)
Mn1−O2	1.875(3)	Mn2−O4	1.879(3)
Mn1−O3	1.874(3)	Mn2−O1	1.898(3)
Mn1−O1	1.926(3)	Mn2−N4	2.092(4)
Mn1−N1	2.099(4)	Mn2−N3	2.201(4)
Mn1−N2	2.181(4)	Mn2−O8	2.612(4)
Bond Angles			
Mn2−O1−Mn1	145.86(17)	Mn2−O1−Nd2	101.79(12)
Mn2−O1−Nd1	93.97(11)	Mn1−O1−Nd2	92.36(11)
Mn1−O1−Nd1	101.15(12)	Nd1−O1−Nd2	128.71(12)

Table 5. Selected Bond Distances (Å) and Angles (deg) for Complex **4**

Bond Lengths			
Gd1−O1	2.417(3)	Mn1−O6	2.597(3)
Gd2−O1	2.461(3)	Mn2−O5	1.874(4)
Mn1−O2	1.866(3)	Mn2−O4	1.879(3)
Mn1−O3	1.871(3)	Mn2−O1	1.898(3)
Mn1−O1	1.918(3)	Mn2−N4	2.100(5)
Mn1−N1	2.088(4)	Mn2−N3	2.198(5)
Mn1−N2	2.175(4)	Mn2−O8	2.579(4)
Bond Angles			
Mn2−O1−Mn1	144.84(19)	Mn2−O1−Gd2	101.63(14)
Mn2−O1−Gd1	93.96(13)	Mn1−O1−Gd2	92.28(13)
Mn1−O1−Gd1	101.59(14)	Gd1−O1−Gd2	129.89(14)

Table 6. Selected Bond Distances (Å) and Angles (deg) for Complex **5**

Bond Lengths			
Tb1−O1	2.404(2)	Mn1−O6	2.584(2)
Tb2−O1	2.440(2)	Mn2−O5	1.875(2)
Mn1−O2	1.866(2)	Mn2−O4	1.875(2)
Mn1−O3	1.868(2)	Mn2−O1	1.897(2)
Mn1−O1	1.920(2)	Mn2−N4	2.091(3)
Mn1−N1	2.097(3)	Mn2−N3	2.205(3)
Mn1−N2	2.180(3)	Mn2−O8	2.568(2)
Bond Angles			
Mn2−O1−Mn1	144.94(12)	Mn2−O1−Tb2	101.83(9)
Mn2−O1−Tb1	93.71(9)	Mn1−O1−Tb2	92.17(8)
Mn1−O1−Tb1	101.49(9)	Tb1−O1−Tb2	130.22(9)

Table 7. Selected Bond Distances (Å) and Angles (deg) for Complex **6**

Bond Lengths			
Dy1−O1	2.393(2)	Mn1−O6	2.568(2)
Dy2−O1	2.434(2)	Mn2−O5	1.875(2)
Mn1−O2	1.865(2)	Mn2−O4	1.878(2)
Mn1−O3	1.869(2)	Mn2−O1	1.8908(19)
Mn1−O1	1.9116(19)	Mn2−N4	2.089(3)
Mn1−N1	2.089(2)	Mn2−N3	2.198(3)
Mn1−N2	2.174(3)	Mn2−O8	2.546(2)
Bond Angles			
Mn2−O1−Mn1	145.35(11)	Mn2−O1−Dy2	101.60(8)
Mn2−O1−Dy1	93.66(8)	Mn1−O1−Dy2	92.11(8)
Mn1−O1−Dy1	101.59(8)	Dy1−O1−Dy2	130.06(8)

one μ_4-O^{2-}, four μ-hep and two μ_3-pivalato ligands, the latter in the η^2:η^1:μ^3-mode. Each Dy is nine coordinate with donors from all ligands mentioned above and two chelating nitrate anions. The coordination polyhedron

Table 8. Selected Bond Distances (Å) and Angles (deg) for Complex **7**

Bond Lengths			
Ho1−O1	2.387(3)	Mn1−O6	2.582(4)
Ho2−O1	2.424(3)	Mn2−O5	1.881(4)
Mn1−O2	1.868(3)	Mn2−O4	1.880(3)
Mn1−O3	1.869(3)	Mn2−O1	1.893(3)
Mn1−O1	1.909(3)	Mn2−N4	2.094(4)
Mn1−N1	2.089(4)	Mn2−N3	2.198(5)
Mn1−N2	2.177(4)	Mn2−O8	2.561(4)
Bond Angles			
Mn2−O1−Mn1	144.84(19)	Mn2−O1−Ho2	101.63(13)
Mn2−O1−Ho1	93.72(13)	Mn1−O1−Ho2	92.30(13)
Mn1−O1−Ho1	101.66(13)	Ho1−O1−Ho2	130.16(14)

Table 9. Selected Bond Distances (Å) and Angles (deg) for Complex **8**

Bond Lengths			
Yb1−O1	2.356(3)	Mn1−O6	2.565(3)
Yb2−O1	2.391(3)	Mn2−O5	1.886(3)
Mn1−O2	1.871(3)	Mn2−O4	1.882(3)
Mn1−O3	1.869(3)	Mn2−O1	1.893(3)
Mn1−O1	1.907(3)	Mn2−N4	2.090(4)
Mn1−N1	2.091(4)	Mn2−N3	2.204(5)
Mn1−N2	2.178(4)	Mn2−O8	2.540(3)
Bond Angles			
Mn2−O1−Mn1	144.17(17)	Mn2−O1−Yb2	101.63(12)
Mn2−O1−Yb1	93.65(12)	Mn1−O1−Yb2	92.27(12)
Mn1−O1−Yb1	101.91(12)	Yb1−O1−Yb2	130.88(12)

may be described as a distorted tricapped trigonal prism or triaugmented triangular prism formed by one μ_4-O^{2-}, two oxygen atoms of the hep^- anion, four oxygen atoms from two nitrate anions acting as η^2 chelating ligands and two oxygen atoms from two pivalate ligands. Both pivalate anions act as η^2:η^1:μ^3 tridentate-bridging ligands between two dysprosium ions and one manganese ion. Intramolecular $\pi-\pi$ stacking interactions between phenyl rings of two parallel 2-(2-hydroxyethyl) pyridine ligands are present. The centroid−centroid distance between these staggered aromatic rings is ~3.519 Å. The Mn ions are in distorted octahedral coordination environments with Jahn−Teller axes (N2−Mn1−O6) and (N3−Mn2−O8) under angle of ~24°. The average Dy−Dy distance in tetrahedral unit of **6** is 4.375 Å, and Mn−Mn is 3.630 Å, respectively. The angles around the (μ_4-O)Mn_2Ln_2 center vary from 92.109(3) to 145.342(6)° consistent with the distorted tetrahedral geometry.

There are no intermolecular $\pi-\pi$ stacking interactions within the structure. However, the aromatic C−H bonds within each molecule form 10 weak C−H···O hydrogen bonds (C···O distances 3.22−3.38 Å) to nitrate oxygens from a total of 6 neighboring molecules.

Magnetic Studies of 1, 4−8. Solid state dc magnetic susceptibility (χ) data for compounds **1**, **4**−**8** were collected in the 1.8−300 K temperature range in a field of 0.1 T. The experimental χT products at room temperature (Figure 3) are all slightly lower than the expected value[20] as can be seen in the Table 11, staying nevertheless in good agreement with the presence of two $S = 2$ Mn^{III} and two Ln^{III} metal ions. On lowering the temperature the χT

(20) Benelli, C.; Gatteschi, D. *Chem. Rev.* **2002**, *102*, 2369.

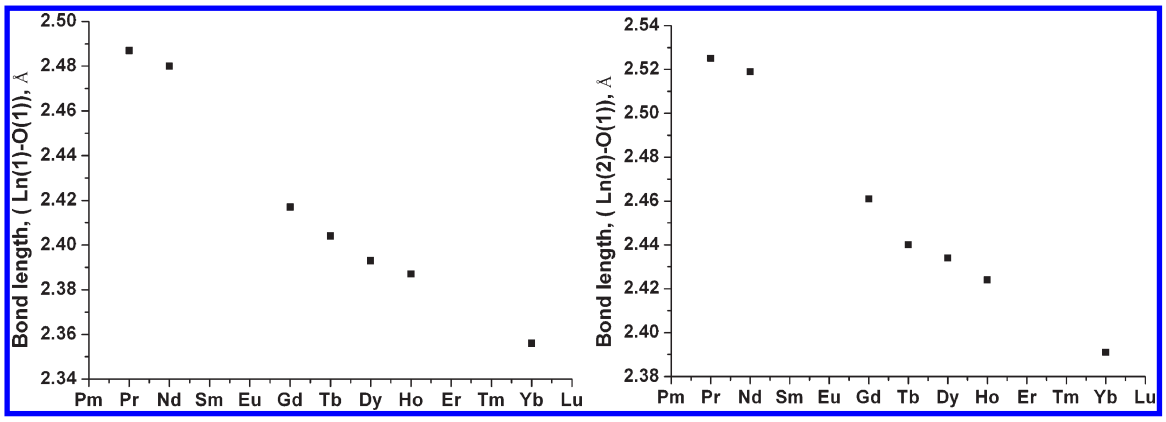

Figure 2. Lanthanide contraction for compounds **2**−**8**.

Table 10. Summary of Structural Characteristics of **1**−**8**

		intermetallic separation (Å)						bond angles (deg)	
complex	ionic radius of Ln^{III}	Ln1−Ln2	Mn1−Mn2	Ln1−Mn1	Ln1−Mn2	Ln2−Mn1	Ln2−Mn2	Mn1−O1−Mn2	Ln1−O1−Ln2
Mn_2Pr_2	1.01	4.518	3.648	3.424	3.230	3.239	3.455	145.62	128.72
Mn_2Nd_2	0.99	4.506	3.656	3.422	3.226	3.233	3.450	145.86	128.71
Mn_2Gd_2	0.94	4.419	3.638	3.374	3.174	3.180	3.397	144.84	129.89
Mn_2Tb_2	0.92	4.395	3.640	3.362	3.157	3.162	3.384	144.94	130.22
Mn_2Dy_2	0.91	4.370	3.630	3.350	3.140	3.150	3.370	145.35	130.06
Mn_2Y_2	0.90	4.368	3.620	3.347	3.144	3.148	3.365	144.26	130.57
Mn_2Ho_2	0.89	4.363	3.625	3.344	3.141	3.145	3.363	144.84	130.16
Mn_2Yb_2	0.86	4.317	3.615	3.322	3.114	3.117	3.335	144.17	130.88

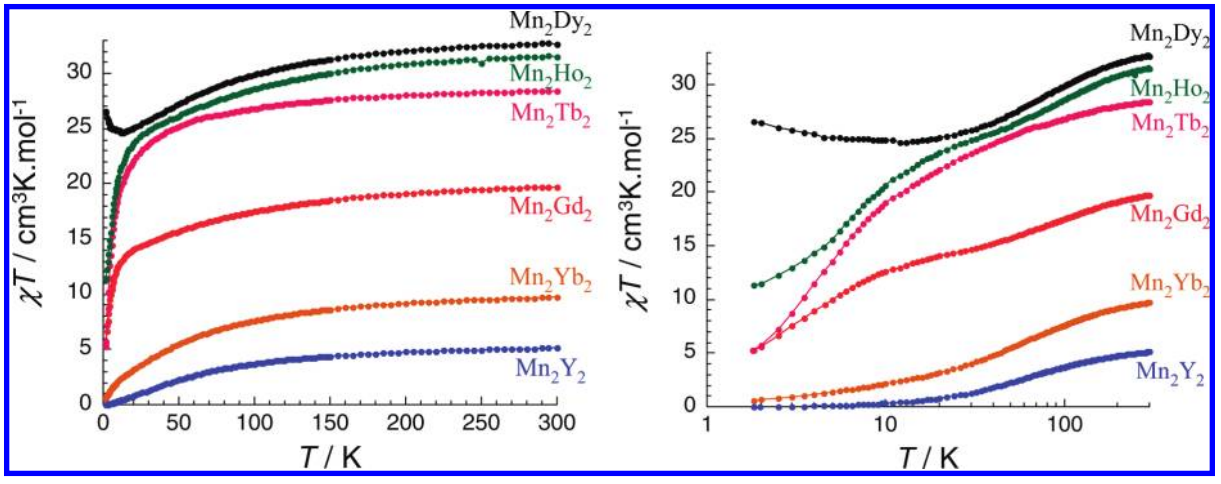

Figure 3. Linear (left) and semilog (right) χT versus T plots for **1**, **4**−**8** at 1000 Oe (with χ being the molar susceptibility defined as M/H).

product decreases down to 1.8 K for all compounds apart from Mn_2Dy_2 which exhibits a minimum at 11 K reaching 24.8 cm^3 K/mol before increasing at 26.7 cm^3 K/mol at 1.8 K. For Mn_2Y_2, Mn_2Gd_2, Mn_2Tb_2, Mn_2Ho_2, and Mn_2Yb_2, the χT products at 1.81 K are 0, 5.2, 5.2, 11.3, and 0.57 cm^3 K/mol, respectively. As can be seen from the semilog plot (Figure 3, right), no clear saturation is observed at low temperature indicating a lack of well-defined ground state apart for Mn_2Y_2 which becomes diamagnetic below 3 K. Such behavior suggests the presence of antiferromagnetic (AF) interactions between spin carriers for all compounds. This does not preclude the presence of ferromagnetic interactions, but does suggest that AF interactions are dominant. On the basis of the low temperature χT values and their extrapolation at 0 K, a $S = 0$ ground state is likely for Mn_2Y_2 and Mn_2Yb_2 while for other compounds it is difficult to be definitive. Nevertheless, for Mn_2Ho_2 and Mn_2Dy_2 the magnetic data shown in Figure 3 strongly suggest non-zero ground states resulting from a ferrimagnetic arrangement of the spins.

Considering the number of magnetic pathways for exchange between spin carriers (Scheme 1) and the difficulty in modeling complexes containing the anisotropic Dy^{III}, Ho^{III}, Tb^{III}, and Yb^{III} ions, the only compound that can be easily modeled is Mn_2Y_2 (**1**) which contains diamagnetic Y^{III} ions. A simple isotropic Heisenberg dimer model of $S = 2$ spins with the following spin Hamiltonian was used:

$$H = -2J_3 S_{MnA} S_{MnB} \quad (1)$$

where J_3 is the exchange interactions in the dimer between the Mn^{III} ions shown in Scheme 1. The application of the van Vleck equation[23] to the Kambe vector coupling

Table 11. Expected and measured χT values for Mn_2Ln_2 at 300 K

compounds	χT (cm^3 K/mol) expected for each Ln at RT[20]	χT (cm^3 K/mol) expected for Mn_2Ln_2 at RT	χT (cm^3 K/mol) measured for Mn_2Ln_2 at RT
Mn_2Y_2, **1**	0	6	5.2
Mn_2Gd_2, **4**	7.875	21.75	19.7
Mn_2Tb_2, **5**	11.815	29.63	28.4
Mn_2Dy_2, **6**	14.17	34.34	32.9
Mn_2Ho_2, **7**	14.075	34.15	31.6
Mn_2Yb_2, **8**	2.57	11.14	9.8

Scheme 1. Magnetic Pathways for Exchange in the $[Mn_2Ln_2O]$ Core

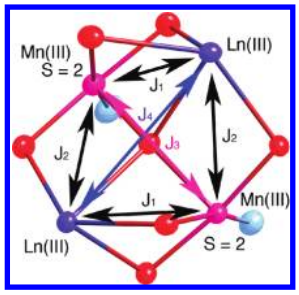

scheme[24] allows a determination of the low field analytical expression of the magnetic susceptibility according to

$$\chi = \frac{g_{av}^2 N\mu_B^2}{k_B T}\frac{2e^{2J_3/k_BT} + 10e^{6J_3/k_BT} + 28e^{12J_3/k_BT} + 60e^{20J_3/k_BT}}{1 + 3e^{2J_3/k_BT} + 5e^{6J_3/k_BT} + 7e^{12J_3/k_BT} + 9e^{20J_3/k_BT}}$$

This model reproduces the experimental data from 300 to 1.8 K very well (Figure 4). The best set of parameters found is: $J_3/k_B = -9.9(1)$ K and $g = 1.99(1)$. The sign of the magnetic interaction confirms the $S = 0$ ground state of this compound (**1**) and also indicates that in the other compounds of this family the arrangement of the Mn^{III} is likely antiferromagnetic. However, it is possible that in these compounds the Mn^{III} spins could be forced to be parallel by the pairwise of $Mn^{III}-Ln^{III}$ interactions (J_1 and J_2) if these are strong enough, although 3d-4f interactions are usually rather weak.

The magnetic behavior of this series of compounds arises from a combination of the $Mn^{III}-Mn^{III}$, $Mn^{III}-Ln^{III}$, and $Ln^{III}-Ln^{III}$ interactions in addition to the intrinsic magnetic properties of the Ln^{III} ions. For the compound Mn_2Gd_2 (**4**) containing isotropic Gd^{III} ions, we can subtract the magnetic contribution of $[Mn_2]$ unit found from the Mn_2Y_2 compound to investigate the interactions of Mn−Gd and Gd−Gd. The profile of the "subtracted" χT versus T curve (Figure 5) suggests an overall antiferromagnetic behavior leading to a nonmagnetic ground state. As is well-known, the bridge angle and the separation between the spin carriers are important parameters in determining the nature of the magnetic interactions in many systems. In compound **4**, the Gd−O−Gd bridge angle at the μ_4-oxo is 129.89° and the separation of Gd···Gd is 4.419 Å. These are similar

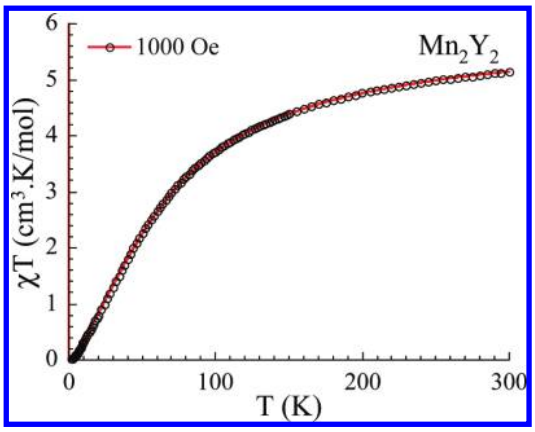

Figure 4. χT versus T plot for **1** at 1000 Oe (with χ being the molar susceptibility defined as M/H). The solid lines represent the best fit obtained with the dinuclear model described in the text.

to those observed in some previously reported dinuclear gadolinium complexes,[21,22] where diamagnetic ground states have been found[21] and it is likely that the Gd−Gd interaction in **4** is also antiferromagnetic. In any case, whatever the nature of the Gd−Gd coupling is it can be expected to be very weak as seen in many pure lanthanide containing complexes.[20] This further suggests that in the other compounds of this family the interaction between the Ln^{III} ions is likely to be weak and antiferromagnetic with the $Mn^{III}-Ln^{III}$ interactions likely to be stronger and the $Mn^{III}-Mn^{III}$ interactions the strongest. The χT versus T curve for Mn_2Dy_2 (**6**) with the contribution from the Mn−Mn gauged from compound **1** subtracted from the data (Figure 5) was plotted. The slight decrease in χT above 20 K originates from the thermal depopulation of the Stark levels resulting from the splitting of the free-ion ground state of Dy^{III}, $^6H_{15/2}$, by the crystal field. The increase of χT at lower temperature below 11 K might originate from weak antiferromagnetic interactions between the Dy^{III} and Mn^{III} ions resulting in a ferrimagnetic arrangement of the spins within the complex. Because of the presence of large orbital contribution from the 4f ions in compounds in **5**−**8**, fitting the data to obtain the $Mn^{III}-Mn^{III}$, $Mn^{III}-Ln^{III}$, and $Ln^{III}-Ln^{III}$ coupling constants is not feasible.

The field dependence (Supporting Information, Figure S2) of the magnetization at low temperature for Mn_2Y_2 (**1**) confirms the $S = 0$ ground state and the field induced excited states are only slightly populated below 7 T. The magnetization for Mn_2Yb_2 (**8**) increases smoothly with the applied dc field without saturation even at 7 T at which point it attains the small value of 2.9 μ_B. This behavior indicates a possible $S = 0$ spin ground state with low lying excited states thermally populated even at 1.8 K. In the case of Mn_2Gd_2 (**4**), the magnetization is close to saturation at 7 T where it attains a value of 13.6 μ_B in good agreement with the presence of two weakly antiferromagnetically coupled $S = 7/2$ Gd^{III} ions. The contribution from the Mn^{III} ions is zero at this temperature because of the AF coupling as seen in Mn_2Y_2 compound. However, the Brillouin function calculated for two isolated $S = 7/2$ spins does not fit the experimental curve found at 1.8 K (Supporting Information, Figure S3). The low field data

(21) (a) Liu, S.; Gelmini, L.; Rettig, S. J.; Thompson, R. C.; Orvig, C. *J. Am. Chem. Soc.* **1992**, *114*, 6081. (b) Costes, J. P.; Dupuis, A.; Laurent, J. P. *Inorg. Chim. Acta* **1998**, *268*, 125.
(22) Costes, J. P.; Clemente-Juan, J. M.; Dahan, F.; Nicodeme, F.; Verelst, M. *Angew. Chem.* **2002**, *114*, 333.
(23) van Vleck, J. H. *The Theory of Electric and Magnetic Susceptibility*; Oxford University Press: New York, 1932.
(24) Kambe, K. *J. Phys. Soc. Jpn.* **1950**, *5*, 48.

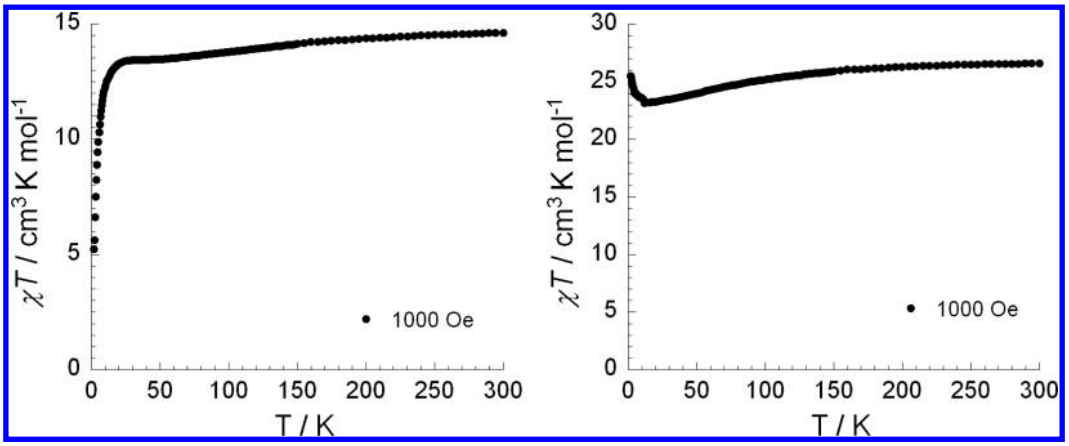

Figure 5. χT versus T plot at 1000 Oe without the magnetic contribution of the [Mn_2] unit for **4** and **6** (with χ being the molar susceptibility defined as M/H).

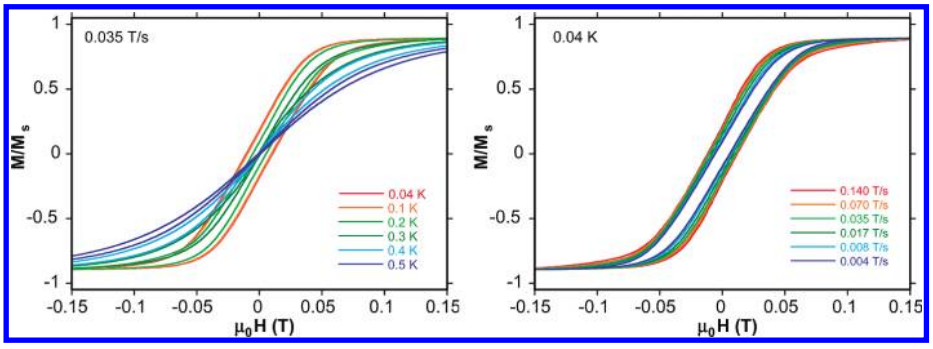

Figure 6. Normalized magnetization (M being normalized at the saturated magnetization M_S) of **6** versus applied field ($\mu_o H$). The loops are shown at different temperatures (left) and at different field sweep rates (right).

are systematically lower than the model suggesting AF interactions between Gd^{III} centers.

The three compounds, Mn_2Tb_2 (**5**), Mn_2Dy_2 (**6**), and Mn_2Ho_2 (**7**), show similar M versus H behavior with a relative rapid increase of the magnetization at low field and then a linear increase without clear saturation. The magnetization at 7 T for Mn_2Tb_2 (**5**), Mn_2Dy_2 (**6**), and Mn_2Ho_2 (**7**) is 10.7, 10.9, and 10.5 μ_B, respectively. The high field linear variation of M suggests the presence a significant anisotropy in these compounds. Moreover, it should be noticed that for Mn_2Tb_2 (**5**) an inflection point on the M versus H is seen around 7000 Oe indicating that the weak antiferromagnetic interactions are overcome by the applied dc field. Therefore, the observed magnetization for Mn_2Tb_2 is certainly influenced by field induced excited states. Population of low-lying excited states at 1.8 K in these compounds makes the presentation of the data in the form of reduced magnetization plots unhelpful.

The ac susceptibility for the compounds was measured to check for any signs of slow relaxation of the magnetization. While Mn_2Y_2 (**1**), Mn_2Gd_2 (**4**), and Mn_2Yb_2 (**8**) do not exhibit any out-of-phase ac signals, Mn_2Tb_2 (**5**), Mn_2Dy_2 (**6**), and Mn_2Ho_2 (**7**) display clear out-of-phase signals indicative of slow relaxation of the magnetization (Supporting Information, Figure S4) below 5 K with a frequency range 0.5−1500 Hz in a 3 Oe field. It can also be noted that these are the three compounds which display significant anisotropy based on the M versus H data. However, with these measurements performed above 1.8 K it is difficult to draw a conclusion on the SMM behavior. Both the temperature and frequency dependence of the ac susceptibility indicate that the relaxation mode is centered at a frequency higher than available in the experimental frequency window (Supporting Information, Figure S5). We took compound **7** as an example and applied a dc field of 2000 Oe and below to see if the relaxation would slow down. In SMMs with a relaxation partially influenced by quantum effects, the application of small dc field removes the state degeneracy and thus the possibility of quantum tunneling in SMMs inducing a slowing down of the magnetization relaxation. For this compound, the relaxation mode is almost unchanged or pushed to higher frequencies under a small dc field (Supporting Information, Figure S6).

To investigate the possible SMM behavior further, single crystal magnetization measurements were performed using an array of micro-SQUIDS at temperatures down to 40 mK.[13] Hysteresis loops with a very small coercivity collected for complex **6** at varying temperatures and sweep rates are shown in Figure 6. These data confirm the presence of slow relaxation of the magnetization as hysteresis effects are clearly seen below 0.3 K at 0.035 T/s. One can also note that the hysteresis is tilted to negative field of about −0.05 T which is indicative of the presence of antiferromagnetic interactions between slowly relaxing magnetic units, which are presumably mediated by the network of intermolecular C−H···O hydrogen bonds (vide infra). Therefore, it was not possible to obtain a reliable value for the energy barrier by magnetization versus time decay data because of the intermolecular interactions.

Conclusions

We have structurally and magnetically characterized a systematic series of isotructural tetranuclear mixed-metal manganese-lanthanide complexes obtained from the reaction of 2-(2-hydroxyethyl) pyridine (hepH) with a preformed $[Mn_6]$ starting material and the appropriate lanthanide nitrate. This new family of Mn-Ln complexes contains members with diamagnetic, isotropic, and anisotropic lanthanides which has enabled us to gauge the influence of the anisotropy of the lanthanide centers by studying the variation of the magnetic properties. The magnetic data presented suggest predominantly antiferromagnetic exchange interactions within complexes. The $Mn^{III}-Mn^{III}$ interactions could be quantified as -9.9 K by studying the Y^{III} analogue where there is no magnetic contribution from the rare earth ions. The compounds containing highly anisotropic lanthanide ions (Tb, Dy, and Ho) show slow relaxation of their magnetization. The investigation of this system can be extended by introducing different substituents onto the pyridine ring.

Acknowledgment. This work was supported by the DFG (Grant SPP 1137 and Center for Functional Nanostructures), MAGMANet (Grant NMP3-CT-2005-515767), the University of Bordeaux, the CNRS, the ANR (NT09_469563, AC-MAGnets project), the Region Aquitaine, and the GIS Advanced Materials in Aquitaine (COMET Project). We thank Dr. Zoltan Gal (Oxford Diffraction) for measuring the data set for **4**.

Supporting Information Available: Structure of **9**. Variable-field magnetization data and plots of the in-phase (χ') and the out-of-phase (χ'') ac susceptibility signals. This material is available free of charge via the Internet at http://pubs.acs.org. CCDC reference numbers 758178−758185. For ESI and crystallographic data in CIF or other electronic format see DOI: 10.1039/b978987j.